Journal of Sound and Vibration 330 (2011) 471–485

Contents lists available at ScienceDirect

Journal of Sound and Vibration

journal homepage: www.elsevier.com/locate/jsvi

Stability and bifurcation of an axially moving beam tuned to three-to-one internal resonances

J.L. Huang [a], R.K.L. Su [b,*], W.H. Li [a], S.H. Chen [a]

[a] Department of Applied Mechanics and Engineering, Sun Yat-sen University, Guangzhou 510275, PR China
[b] Department of Civil Engineering, The University of Hong Kong, Pokfulam, Hong Kong, PR China

ARTICLE INFO

Article history:
Received 28 December 2009
Received in revised form
30 April 2010
Accepted 30 April 2010
Handling Editor: L.N. Virgin
Available online 16 September 2010

ABSTRACT

This study analyzed the nonlinear vibration of an axially moving beam subject to periodic lateral force excitations. Attention is paid to the fundamental and subharmonic resonances, since the excitation frequency is close to the first two natural frequencies of the system. The incremental harmonic balance (IHB) method was used to evaluate the nonlinear dynamic behaviour of the axially moving beam. The stability and bifurcations of the periodic solutions for given parameters were determined by the multivariable Floquet theory using Hsu's method. The solutions obtained from the IHB method agreed very well with those obtained from numerical integration. Furthermore, numerical examples are given to illustrate the effects of the three-to-one internal resonance on the response of the system.

1. Introduction

Axially moving systems are widely used in engineering applications for conveying materials or in power transmissions, such as magnetic tapes, power transmission belts and band saw blades. Such systems, which can be modelled as either string-like or beam-like systems, have been investigated in the past by many researchers [1,2]. Wickert and Mote Jr. [3] used an eigenfunction method to analyze the response of axially moving strings and beams subjected to arbitrary excitation and initial conditions. Wickert [4] analyzed the nonlinear vibration and bifurcation of axially moving beams through the Krylov–Bogoliubov–Mitropolsky asymptotic method. Pellicano and Vestroni [5,6] studied the nonlinear dynamics of a simply supported axially moving beam using a high-dimensional discrete model obtained from the Galerkin procedure. These authors also investigated the effect of pulley eccentricity on the vibration of an axially moving belt by experimental and theoretical analysis [7]. In many studies, the method of multiple scales is applied to analyze the nonlinear vibration of axially moving strings or beams. Öz et al. [8] and Öz [9] applied the method of multiple scales to study the nonlinear vibrations and stability of axially moving beams and tensioned pipes conveying fluid with time-dependent velocity. Chen and Yang [10,11] used the method of multiple scales to calculate the steady-state response of axially moving viscoelastic beams with time-dependent velocity and investigated stability in transverse parametric vibration. Recently, Sze et al. [12] investigated the forced response of an axially moving beam with internal resonance using the IHB method, which is an efficient and reliable method for treating the vibration of strong nonlinear systems [13–15].

Internal resonance has been found in many engineering problems in which the natural frequencies of the system are commensurable. When internal resonance occurs, the two vibration modes may react with each other, and energy may be

* Corresponding author. Tel.: +852 2859 2648; fax: +852 2559 5337.
E-mail address: klsu@hkucc.hku.hk (R.K.L. Su).

0022-460X/$ - see front matter © 2010 Elsevier Ltd. All rights reserved.
doi:10.1016/j.jsv.2010.04.037

transferred between the two resonant modes. Chin and Nayfeh [16] investigated three-to-one internal resonance in hinged–clamped beams subject to a primary excitation in either its first or its second mode. They used the method of multiple scales to directly solve the governing nonlinear partial differential equation, a shooting technique to calculate limit cycles of the modulation equations and the Floquet theory to ascertain their stability. Abe et al. [17] also used the method of multiple scales to analyze internal resonance between two symmetric mode responses of simply supported rectangular laminated plates. They reported that the two-mode response near the primary resonance of the second mode loses its stability via a Hopf bifurcation, giving rise to a quasi-periodic response. The two modes of the axially moving beam needed to be studied simultaneously in order to realise the dynamic behaviour of the system. In this regard, Riedel and Tan [18] studied the coupled and forced responses of an axially moving strip with internal resonance when the force frequency was near the first natural frequency. The method of multiple scales was used to perform the perturbation analysis and to determine the frequency-response numerically for both low and high speed conditions. Suweken and Van Horssen [19] investigated complicated dynamical behaviour for sum-type and difference-type internal resonances on the transverse vibrations of a conveyor belt with time-varying velocity; the stability properties of the belt system were demonstrated. Sze et al. [12] also studied the nonlinear vibration of the system with the IHB method. They observed that the internal resonances are rich and complicated.

This paper is focused on the stability and bifurcation of periodic solutions of the axially moving beam with internal resonance when the excitation frequency, Ω, is near the first two natural frequencies, ω_1 and ω_2. Two nonlinear ordinary differential equations can be derived through Hamilton's Principle and discretised through Galerkin's method. Then, the IHB method is employed to solve the equations to obtain the frequency response curves of the axially moving beam. Based on the Floquet theorem, the stability and bifurcation of the periodic solutions are determined by observing the movement of the eigenvalues of the transition matrix in the complex plane. The transition matrix can be evaluated by using Hsu's method [20–22]. The periodic, quasi-periodic and chaotic motions are investigated by numerical integration and represented in terms of the time histories, phase plane plots, Poincaré sections, Fourier spectra and Lyapunov exponents. Some resonance curves are presented and discussed.

2. System model and associated equations of motion

Fig. 1 shows a beam passing through two simple supports at constant transport velocity V with a transverse force. The properties of the beam include its cross-sectional area, A, mass density, ρ and flexural rigidity, EI. The beam is tensioned by force, P, and it oscillates in the X–Z-plane with the transverse displacement denoted by $W(X, T)$, where T denotes time. Furthermore, the beam is excited by $Q(X, T)$, the vertical dynamic load. From the previous studies, the natural frequencies of the transverse vibration differ greatly from that of the longitudinal vibration [4], and the coupling effect between the two vibrations is weak. Hence, in this study, the effects of longitudinal vibration in the moving beam are neglected.

The governing equation of the axially moving beam subject to a transverse harmonic excitation can be expressed non-dimensionally as [4]

$$w_{,tt}+2vw_{,xt}+(v^2-1)w_{,xx}-\tfrac{3}{2}v_1^2w_{,x}^2w_{,xx}+v_f^2w_{,xxxx}=F\cos\boldsymbol{\Omega}t \tag{1}$$

subject to the boundary conditions

$$w(0,t)=w(1,t)=0,\quad w_{,xx}(0,t)=w_{,xx}(1,t)=0 \tag{2}$$

in which $w=W/L,\ x=X/L,\ t=T\sqrt{P/\rho AL^2}$.

$$v=V/\sqrt{P/\rho A},\quad v_1=\sqrt{EA/P},\quad v_f=\sqrt{EI/PL^2}\ \text{and}\ F=QL/P$$

where $w(x, t)$ is the non-dimensional lateral deflection, v is the non-dimensional constant transport velocity, v_1 is the non-dimensional longitudinal stiffness parameter, v_f is the non-dimensional flexural stiffness parameter, F is the non-dimensional lateral force and Ω is the non-dimensional excitation frequency whose physical counterpart is $\boldsymbol{\Omega}\sqrt{P/\rho AL^2}$.

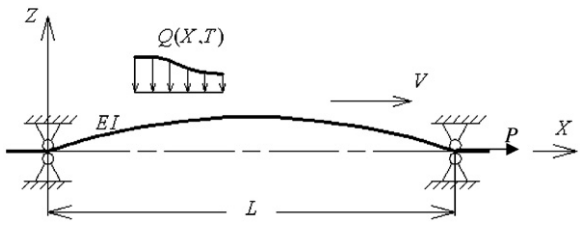

Fig. 1. Schematic diagram for an axially moving beam.

The following separable solutions, in terms of admissible functions and the dynamic load $F(x, t)$, are assumed to be

$$w(x,t) = \sum_{j=1}^{n} q_j(t)\sin(j\pi x) \tag{3}$$

$$F(x,t) = \sum_{j=1}^{n} f_j \sin(j\pi x) \tag{4}$$

By substituting Eqs. (3) and (4) into Eq. (1), multiplying all the terms by $\sin(i\pi x)$ and integrating the resulting equation from x=0 to 1, the following second-order ordinary differential equations can be obtained:

$$\sum_{j=1}^{n} M_{ij}\ddot{q}_j + \sum_{j=1}^{n} G_{ij}\dot{q}_j + \sum_{j=1}^{n} K_{ij}q_j + \sum_{j=1}^{n}\sum_{k=1}^{n}\sum_{l=1}^{n} K_{ijkl}q_j q_k q_l = f_j \cos \boldsymbol{\Omega} t, \quad i = 1,2,\ldots,n \tag{5}$$

where $\dot{q}_j = dq_j/dt$ and $\ddot{q}_j = d^2q_j/dt^2$. Moreover, M_{ij}, G_{ij}, K_{ij} and K_{ijkl} are the mass, gyroscopic, linear stiffness and cubic stiffness coefficients in the discretized equations, respectively.

Eq. (5) can then be rewritten in matrix form as

$$M\ddot{\mathbf{q}} + G\dot{\mathbf{q}} + \mathrm{Kq} + \mathbf{K}_3(\mathbf{q})\mathbf{q} = \mathrm{F}\cos \boldsymbol{\Omega} t \tag{6}$$

where $\mathbf{q} = [q_1, q_2,\ldots,q_n]^T$, M, Gand Kare the mass, gyroscopic and linear stiffness matrices, respectively, $K_3(q)$ is the cubic nonlinear stiffness matrix and $\mathbf{F} = [f_1,f_2,\ldots,f_n]^T$ is the amplitude matrix of the disturbed harmonic excitation.

By introducing the new non-dimensional time variable, τ

$$\tau = \boldsymbol{\Omega} t \tag{7}$$

Eq. (6) becomes

$$\boldsymbol{\Omega}^2 \mathrm{Mq}'' + \boldsymbol{\Omega}\mathrm{Gq}' + \mathrm{Kq} + \mathbf{K}_3(\mathbf{q})\mathbf{q} = \mathbf{F}\cos\tau \tag{8}$$

in which the prime denotes differentiation with respect to τ.

3. IHB method for the axially moving beam

Among the methods of solving ordinary differential equations, the IHB method is an efficient and reliable method for treating strongly nonlinear vibrational systems. It was developed and successfully applied to the analysis of periodic nonlinear structural vibrations and related problems.

The first step of the IHB method is an incremental method (Newton–Raphson procedure) to linearise the incremental differential equation, Eq. (8). Let q_{j0} and ω_0 denote a state of vibration; the neighbouring state can be express by adding the corresponding increments as follows:

$$q_j = q_{j0} + \Delta q_j, \quad j = 1,2,\ldots,n, \quad \boldsymbol{\Omega} = \omega_0 + \Delta\omega \tag{9}$$

Substituting Eq. (9) into Eq. (8) and neglecting the higher-order terms yields the following incremental equation in matrix form:

$$\omega_0^2\mathbf{M}\Delta\mathbf{q}'' + \omega_0\mathbf{G}\Delta\mathbf{q}' + \mathbf{K}\Delta\mathbf{q} + 3\mathbf{K}_3\Delta\mathbf{q} = \overline{\mathbf{R}} - (2\omega_0\mathbf{M}\mathbf{q}''_0 + \mathbf{G}\mathbf{q}'_0)\Delta\omega \tag{10}$$

$$\overline{\mathbf{R}} = \mathbf{F}\cos\tau - (\omega_0^2\mathbf{M}\mathbf{q}''_0 + \omega_0\mathbf{G}\mathbf{q}'_0 + \mathbf{K}\mathbf{q}_0 + \mathbf{K}_3\mathbf{q}_0) \tag{11}$$

in which

$$\mathbf{q}_0 = [q_{10},q_{20},\ldots,q_{n0}]^T, \quad \Delta\mathbf{q}_0 = [\Delta q_1,\Delta q_2,\ldots,\Delta q_n]^T$$

and $\overline{\mathbf{R}}$ is a corrective vector which goes to zero when the numerical solution is exact.

The second step of the IHB method is the harmonic balance procedure. For a periodic excitation force and if Eq. (8) is odd, a periodic solution can be obtained by expanding q_{j0} in a truncated finite Fourier series and using the Galerkin procedure. Thus, we can assume

$$q_{j0} = \sum_{k=1}^{n_c} a_{jk}\mathbf{cos}(2k-1)\tau + \sum_{k=1}^{n_s} b_{jk}\mathbf{sin}(2k-1)\tau = \mathbf{C}\mathbf{A}_j \tag{12}$$

where

$$\mathbf{C} = [\cos\tau,\cos 3\tau\ldots,\cos(2n_c-1)\tau,\sin\tau,\sin 3\tau,\ldots,\sin(2n_s-1)\tau]$$

$$\mathbf{A}_j = [a_{j1},a_{j2},\ldots,a_{jn_c},b_{j1},b_{j2},\ldots,b_{jn_s}]^T$$

and a_{jk}, b_{jk} are the Fourier coefficients, and n_c, n_s are the numbers of the cosine and sine harmonic terms, respectively.

The increment Δq_j can also be expanded in a Fourier series as shown below:

$$\Delta q_{j0} = \sum_{k=1}^{n_c} \Delta a_{jk} \cos(2k-1)\tau + \sum_{k=1}^{n_s} \Delta b_{jk} \sin(2k-1)\tau = \mathbf{C}\Delta\mathbf{A}_j \tag{13}$$

where $\Delta\mathbf{A}_j = [\Delta a_{j1}, \Delta a_{j2}, \ldots, \Delta a_{j\,n_c}, \Delta b_{j1}, \Delta b_{j2}, \ldots, \Delta b_{j\,n_s}]^T$. Hence, the vectors of the unknown and their increments can be expressed, respectively, using the Fourier coefficient vector, A, and its increment, ΔA, as

$$\mathbf{q}_0 = \mathrm{SA}, \quad \Delta\mathbf{q}_0 = \mathbf{S}\Delta\mathbf{A} \tag{14}$$

Here, $\mathbf{S} = \mathrm{diag}(\mathbf{C},\mathbf{C},\ldots,\mathbf{C})$, $\mathbf{A} = [\mathbf{A}_1,\mathbf{A}_2,\ldots,\mathbf{A}_n]^T$ and $\Delta\mathbf{A} = [\Delta\mathbf{A}_1,\Delta\mathbf{A}_2,\ldots,\Delta\mathbf{A}_n]^T$.

Substituting Eq. (14) into Eq. (10) and applying the Galerkin procedure in order to balance the harmonics yields

$$\begin{aligned}\int_0^{2\pi} \delta(\Delta\mathbf{q})^T[\omega_0^2\mathbf{M}\Delta\mathbf{q}'' + \omega_0\mathbf{G}\Delta\mathbf{q}' + \mathbf{K}\Delta\mathbf{q} + 3\mathbf{K}_3\Delta\mathbf{q}]\,\mathrm{d}\tau \\ = \int_0^{2\pi} \delta(\Delta\mathbf{q})^T[\overline{\mathbf{R}} - (2\omega_0\mathbf{M}\mathbf{q}''_0 + \mathbf{G}\mathbf{q}'_0)\Delta\omega]\,\mathrm{d}\tau\end{aligned} \tag{15}$$

One can easily obtain a set of linear equations in terms of ΔA and $\Delta\omega$:

$$\mathbf{K}\Delta\mathbf{A} = \mathbf{R} - \mathbf{R}_{mc}\Delta\omega \tag{16}$$

where

$$\begin{aligned}\mathbf{K} &= \int_0^{2\pi} \mathbf{S}^T[\omega_0^2\mathrm{MS}'' + \omega_0\mathrm{GS}' + (\mathbf{K} + 3\mathbf{K}_3)\mathbf{S}]\,\mathrm{d}\tau \\ \mathbf{R} &= \int_0^{2\pi} \mathbf{S}^T[\mathbf{F}\cos\tau - \omega_0^2\mathrm{MS}'' - \omega_0\mathrm{GS}' - (\mathbf{K} + \mathbf{K}_3)\mathbf{S}]\,\mathrm{d}\tau\mathbf{A} \\ \mathbf{R}_{mc} &= \int_0^{2\pi} \mathbf{S}^T(2\omega_0\mathbf{MS}'' + \mathbf{GS}')\,\mathrm{d}\tau\mathbf{A}\end{aligned}$$

The solution process begins with a guessed solution. The nonlinear frequency-response curve is then solved point-by-point by incrementing the frequency Ω, or incrementing components of the coefficient vector, $\mathbf{A}$. The Newton–Raphson iterative method can be employed, and the solution of the differential equation can be found.

4. Stability analysis

When the steady-state solution of the axially moving system is obtained, the stability of the given solution can be investigated by adding a small perturbation, Δq, onto q_0,

$$\mathrm{q} = \mathrm{q}_0 + \Delta\mathrm{q} \tag{17}$$

Substituting Eq. (17) into Eq. (8), noting that q_0 satisfies Eq. (8), and neglecting the nonlinear incremental terms, one can obtain

$$\boldsymbol{\Omega}^2\mathrm{M}\Delta\mathrm{q}'' + \boldsymbol{\Omega}\mathrm{G}\Delta\mathrm{q}' + (\mathrm{K} + 3\mathrm{K}_3)\Delta\mathrm{q} = 0 \tag{18}$$

Eq. (18) is the perturbed equation: i.e., perturbed from the known solution q_0. The stability of the steady-state solutions then corresponds to the stability of the solutions of Eq. (18), which is a linear ordinary differential equation with periodic coefficients in K_3. These stability characteristics can be studied using the multivariable Floquet theory.

Furthermore, Eq. (18) can be rewritten in the state space form

$$\mathrm{X}' = \mathrm{Q}(\tau)\mathrm{X} \tag{19}$$

where $\mathbf{Q} = \begin{bmatrix} 0 & \mathbf{I} \\ \mathbf{Q}_{21} & -(1/\boldsymbol{\Omega})\mathbf{M}^{-1}\mathbf{G} \end{bmatrix}$, $\mathbf{X} = [\Delta\mathbf{q},\Delta\mathbf{q}']^T$ and $\mathbf{Q}_{21} = -1/\boldsymbol{\Omega}^2\,\mathbf{M}^{-1}(\mathbf{K} + 3\mathbf{K}_3)$. Since each component of q_0 is a periodic function of τ with a period $T = 2\pi$, each element of Q_{21} is also a periodic function with the same period T.

For Eq. (19), there exists a fundamental set of solutions

$$y_k = [y_{1k}, y_{2k}, \ldots, y_{Nk}]^T, \quad k = 1, 2, \ldots, N \tag{20}$$

where $N = 2n$. This fundamental set can be expressed in a matrix called a fundamental matrix solution, i.e.,

$$\mathbf{Y} = \begin{bmatrix} y_{11} & y_{12} & \cdots & y_{1N} \\ y_{21} & y_{22} & \cdots & y_{2N} \\ \vdots & \vdots & \cdots & \vdots \\ y_{N1} & y_{N2} & \cdots & y_{NN} \end{bmatrix} \tag{21}$$

$\mathbf{Y}$ satisfies the matrix equation

$$\mathbf{Y}' = \mathbf{Q}(\tau)\mathbf{Y} \tag{22}$$

where $Q(\tau+T)=Q(\tau)$ is the periodic matrix and $Y(\tau+T)$ is a fundamental matrix solution. Therefore, Y can be expressed by

$$\mathbf{Y}(\tau+T)=\mathrm{PY}(\tau) \tag{23}$$

where P is a non-singular constant matrix called the transition matrix.

The Floquet theory states that the stability criteria for the system are related to the eigenvalues λ_i of the matrix P, or the real of part of the characteristic exponents. The solution of Eq. (19) approaches zero as $\tau\to\infty$ if all the moduli of the eigenvalues of P are less than 1. Otherwise, the motion is unbounded, and the solution is unstable.

Among the various methods of approximating the transition matrix, Friedmann et al. [20] summarised that the most efficient procedures is the one developed by Hsu [21,22] and Hsu and Cheng [23]. The method consists of evaluating the transition matrix by dividing a period into a number of equal parts and considering the equations over each interval to be a set of equations with constant coefficients. Friedmann summarised this method and gave a clear and concise formulation. In this paper, only the final formula is presented. Suppose each period, T, is divided into N_k intervals denoted by τ_k, and the kth interval is denoted by $\Delta_k=\tau_k-\tau_{k-1}$. In the kth interval, the periodic coefficient matrix, $Q(\tau)$, is replaced by a constant matrix, Q_k, defined by

$$\mathbf{Q}_k=\frac{1}{\Delta_k}\int_{\tau_{k-1}}^{\tau_k}\mathbf{Q}(\zeta)\mathrm{d}\zeta \tag{24}$$

Finally, the transition matrix is given in the form

$$\mathbf{P}=\mathbf{Y}(T)=\prod_{i=1}^{N_k}\left[\mathbf{I}+\sum_{j=1}^{N_j}\frac{(\Delta_i\mathbf{Q}_i)^j}{j!}\right] \tag{25}$$

where N_j is the number of the Taylor series.

For numerical evaluation of Eqs. (24) and (25), the algorithms given in Cheung et al. [24] are recommended.

5. Results and discussion

When considering the vibrations of two transverse degrees of freedom, i.e., $n=2$, and introducing model damping terms (μ_{11} and μ_{22}) for the forced responses of the system, Eq. (6) becomes

$$\begin{aligned}\ddot{q}_1+\mu_{11}\dot{q}_1-\mu_{12}\dot{q}_2+k_{11}q_1+k_{12}q_1q_2^2+k_{13}q_1^3&=f_1\cos\boldsymbol{\Omega}t\\ \ddot{q}_2+\mu_{21}\dot{q}_1+\mu_{22}\dot{q}_2+k_{21}q_2+k_{22}q_2q_1^2+k_{23}q_2^3&=f_2\cos\boldsymbol{\Omega}t\end{aligned} \tag{26}$$

where

$$\mu_{12}=\mu_{21}=16\nu/3,\quad k_{11}=(\nu_f^2\pi^2-\nu^2+1)\pi^2,\quad k_{12}=3\nu_1^2\pi^4,\quad k_{13}=k_{12}/8$$

$$k_{21}=4(4\nu_f^2\pi^2-\nu^2+1)\pi^2,\quad k_{22}=k_{12},\quad k_{23}=2k_{12}$$

Here, Ω is the excitation frequency. It should be noted that μ_{12} and μ_{21} are the gyroscopic coefficients that provide an internal damping effect to the system, and μ_{11} and μ_{22} arise from external viscous damping.

Riedel and Tan [18] investigated the internal resonance response of an axially moving strip. Following their chosen system parameters, which are typical for a belt-drive system,

$$\nu_1^2=1124,\quad \nu_f^2=0.03\quad\text{and}\quad \nu=0.6.$$

This set of parameters will be employed throughout this section. From these parameters, one can calculate

$$\mu_{12}=\mu_{21}=3.2,\quad k_{11}=9.23882,\quad k_{12}=3372\pi^4,\quad k_{13}=421.5\pi^4$$

$$k_{21}=72.0226,\quad k_{22}=3372\pi^4,\quad k_{23}=6744\pi^4$$

By dropping the nonlinear terms, the linear natural frequencies ω_1 and ω_2 can be solved from the following equation:

$$\omega^4-(k_{11}+k_{21}+\mu_{12}\mu_{21})\omega^2+k_{11}k_{21}=0 \tag{27}$$

yielding $\omega_1=2.82232$, $\omega_2=9.13980$. For a cubic nonlinearity system, internal resonance usually occurs between two transverse modes when the natural frequency is $\omega_2\approx 3\omega_1$.

5.1. The case of Ω near ω_1

In this case, when the forcing frequency, Ω, is near the first natural frequency, ω_1, $f_2=0$ should be set in Eq. (26). In the solution process, it may be assumed that $n_c=n_s=8$ in Eq. (13) and q_1, q_2 in Eq. (12) can be expressed as

$$\begin{aligned}q_1&=A_{11}\cos(\tau+\phi_{11})+A_{12}\cos(3\tau+\phi_{12})+\cdots\\ q_2&=A_{21}\cos(\tau+\phi_{21})+A_{22}\cos(3\tau+\phi_{22})+\cdots\end{aligned} \tag{28}$$

where

$$A_{jk}=\sqrt{a_{jk}^2+b_{jk}^2},\quad \phi_{jk}=\tan^{-1}(-b_{jk}/a_{jk}),\quad j=1,2,\quad k=1,2,\ldots,8$$

Fig. 2 shows the frequency-response curves of the axially moving beam with f_1=0.0055 and μ_{11}=μ_{22}=0.04 as the excitation frequency ratio Ω/ω_1 varies over the range 0.6–2.0. The ordinate is the non-dimensional amplitude of each mode, and the abscissa is Ω/ω_1, which corresponds to the non-dimensional excitation frequency ratio. The response curves exhibit hardening spring type behaviours. Fig. 2(a) shows the $\boldsymbol{\Omega}/\omega_1 \sim A_{11}$ curve and (b) shows the $\boldsymbol{\Omega}/\omega_1 \sim A_{22}$ curve, where A_{11} and A_{22}, defined in Eq. (28), are the amplitudes of the first harmonic terms of the first variable, q_1, and the second harmonic terms of the second variable, q_2, respectively. In these figures, the solid and dashed lines represent the stable and unstable solutions evaluated from the IHB method, respectively. The small circles represent the solutions obtained from the numerical integration of the perturbation in Eq. (26) using the fourth-order Runge–Kutta method. It can be observed that the results from the IHB method and numerical integration agree well with each other. Figs. 2(c) and (d) show detailed resonant regions obtained by enlarging Figs. 2(a) and (b), respectively.

In Fig. 2, as Ω/ω_1 increases from a small value of 0.6, the amplitude A_{11} rises first through point '*A*', and it then drops slowly at the local maximum '*B*' ($\boldsymbol{\Omega}/\omega_1=1.2123$) until point '*C*' ($\boldsymbol{\Omega}/\omega_1=1.2260$). Alternatively, the amplitude A_{22} rises all the way over the same frequency range. From points '*B*' to '*C*', the system exhibits energy transition from the first response mode to the second response mode due to the internal resonance. At point '*C*', a saddle-node bifurcation occurs resulting in the response becoming unstable, which is evidenced by one pair of complex conjugate Floquet multiplies as shown in Table 1 leaving the unit circle away from the real axis. For decreasing Ω/ω_1 beyond point '*C*', the system response is unstable until another saddle-node bifurcation point '*D*' ($\boldsymbol{\Omega}/\omega_1=1.1664$). In the small stable response region from point '*D*' to point '*E*' ($\boldsymbol{\Omega}/\omega_1=1.1678$), the amplitude A_{11} rises while A_{22} drops with increasing Ω/ω_1 until $A_{22}\approx A_{11}$. In this region, energy is transmitted back from the second response mode to the first response mode. In between points '*D*' and '*E*', there are three stable responses and two unstable responses. Figs. 3(a, b) show the phase planes of the three stable period solutions and two unstable solutions obtained (one of the unstable solution cannot be seen in the figure because it is very close to one of the stable solutions) from the IHB method with an excitation frequency ratio of $\boldsymbol{\Omega}/\omega_1=1.1665$. The cross marks '$\times$' represent the solutions obtained from numerical integration. Again, the solutions from the IHB method and numerical integration show very good agreement. By increasing Ω/ω_1, the system response loses its stability via a Hopf bifurcation at point '*E*' in Fig. 2(d), which is indicated by one pair of complex conjugate Floquet multiplies as shown in Table 2 crossing the unit circle, and retains its stability via a reverse Hopf bifurcation at point '*F*' ($\boldsymbol{\Omega}/\omega_1=1.2380$). Then,

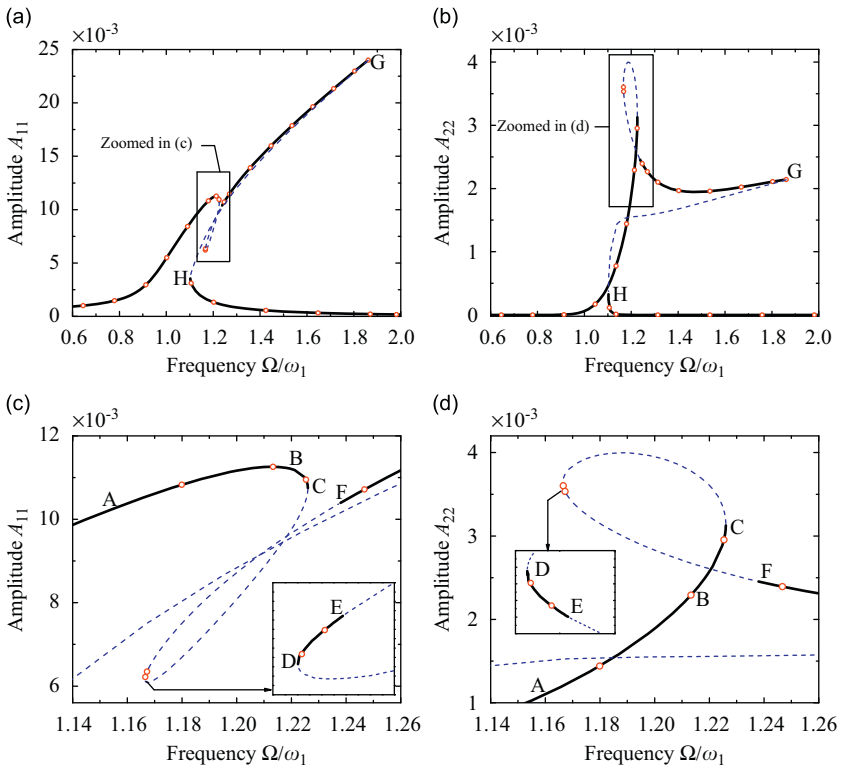

Fig. 2. Response curves as $\omega_2\approx 3\omega_1$, $\Omega\approx\omega_1$ with $f_1=0.0055$, $\mu_{11}=\mu_{22}=0.04$: (a)$\boldsymbol{\Omega}/\omega_1\sim A_{11}$; (b) $\boldsymbol{\Omega}/\omega_1\sim A_{22}$; (c) enlargement of the area highlighted in (a) and (d) enlargement of the area highlighted in (b). ——— IHB stable, - - - - IHB unstable; ○ numerical integration (NI).

the system response encounters a saddle-node bifurcation at point '*G*' ($\boldsymbol{\Omega}/\omega_1 = 1.8610$), resulting in a jump of the response to the smaller stable solution. By decreasing Ω/ω_1 from 2.0 in the smaller stable solution, the system response loses its stability via a saddle-node bifurcation at point '*H*' ($\boldsymbol{\Omega}/\omega_1 = 1.0260$), resulting in a jump of the response to the other stable solution.

It is noted that there exists quasi-periodic or chaotic vibration as Ω/ω_1 decreases from the Hopf bifurcation point '*F*' to 1.1952. Figs. 4 and 5 show the time histories, Fourier spectra, phase plane diagrams and Poincaré sections for the excitation frequency ratios at two points $\boldsymbol{\Omega}/\omega_1 = 1.2333$ and $\boldsymbol{\Omega}/\omega_1 = 1.2066$, which are quasi-periodic and chaotic vibrations, respectively. In Figs. 4 and 5(a,b), the results show that energy is continuously being exchanged between the two modes, resulting in a beating phenomenon. For $\boldsymbol{\Omega}/\omega_1 = 1.2333$, the Lyanpunov exponents are 1.425810-4, -0.02047, -0.02982, -0.02993 and the largest Lyapunov exponent is a very small value, which can be taken to be zero for a quasi-periodic vibration. For $\boldsymbol{\Omega}/\omega_1 = 1.2066$, the Lyanpunov exponents are 0.00298, 8.7382510-5, -0.03935, -0.04378 and the largest Lyapunov exponent is positive, which confirms its chaotic nature. As the excitation frequency ratio decreases slightly close to 1.1952, the system response moves far away from the quasi-periodic or chaotic response and jumps to a stable periodic response. Fig. 6 shows the time histories of q_1 and q_2 at $\boldsymbol{\Omega}/\omega_1 = 1.1951$. It can be seen that the two modes, q_1 and q_2, jump from a quasi-periodic vibration to a stable periodic vibration after a finite time.

A quasi-periodic response bifurcates into a chaotic response when Ω/ω_1 increases from the other Hopf bifurcation point '*E*' to 1.16911. The stable response loses its stability via the Hopf bifurcation point 'E' and becomes a quasi-periodic vibration, as shown in Fig. 7(a). Then, the quasi-periodic vibration undergoes a sequence of period doubling bifurcations, as shown in Fig. 7(b) and (c), eventually resulting in chaotic vibration. The chaotic attractor is observed in Fig. 7(d), and the Lyapunov exponents computed for these parameter values are 0.00781, 4.73918×10^{-5}, -0.04171 and -0.04618. The largest Lyapunov exponent is positive, which confirms its chaotic nature. As the excitation frequency ratio increases slightly near the boundary crises, the system response moves far away from the chaotic attractor and jumps to a stable periodic response. Fig. 8 shows the time histories of q_1 and q_2 at $\boldsymbol{\Omega}/\omega_1 = 1.16967$. The amplitude of the first mode, q_1, rises for a finite period of time and jumps to a stable periodic response, whereas the amplitude of the second mode, q_2, drops and jumps to a stable periodic response.

Table 1
Floquet multiplies with force frequency Ω near point '*C*'.

Frequency, Ω/ω_1	λ_1, λ_2	$\lvert\lambda_1\rvert = \lvert\lambda_2\rvert$	λ_3, λ_4	$\lvert\lambda_3\rvert$, $\lvert\lambda_4\rvert$
1.22557	$0.80383 \pm 0.54730i$	0.97246	$0.94943 \pm 0.11403i$	0.95626, 0.95626
1.22595	$0.81592 \pm 0.53001i$	0.97295	$0.95345 \pm 0.06682i$	0.95579, 0.95579
Point '*C*' 1.22601	$0.82559 \pm 0.51550i$	0.97331	1.01303, 0.90112	1.01303, 0.90112
1.22554	$0.84227 \pm 0.48881i$	0.97383	1.09885, 0.82980	1.09885, 0.82980
1.22219	$0.86893 \pm 0.44011i$	0.97403	1.20373, 0.75691	1.20373, 0.75691

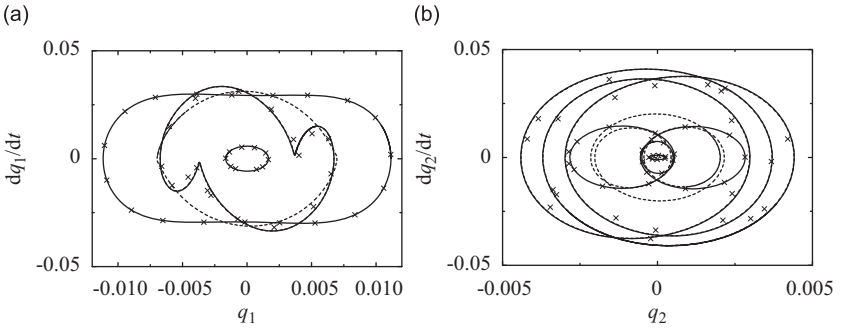

Fig. 3. Multiple responses at $\boldsymbol{\Omega}/\omega_1 = 1.1665$.

Table 2
Floquet multiplies with force frequency Ω near point '*E*'.

Frequency, Ω/ω_1	λ_1, λ_2	$\lvert\lambda_1\rvert = \lvert\lambda_2\rvert$	λ_3, λ_4	$\lvert\lambda_3\rvert = \lvert\lambda_4\rvert$
1.16761	$0.90528 \pm 0.23006i$	0.93406	$0.96641 \pm 0.22378i$	0.99198
1.16775	$0.97299 \pm 0.23032i$	0.99988	$0.89794 \pm 0.22906i$	0.92669
Point '*E*' 1.16782	$0.97569 \pm 0.23297i$	1.00311	$0.89486 \pm 0.22903i$	0.92371
1.16796	$0.97975 \pm 0.23736i$	1.00809	$0.89002 \pm 0.22960i$	0.91916

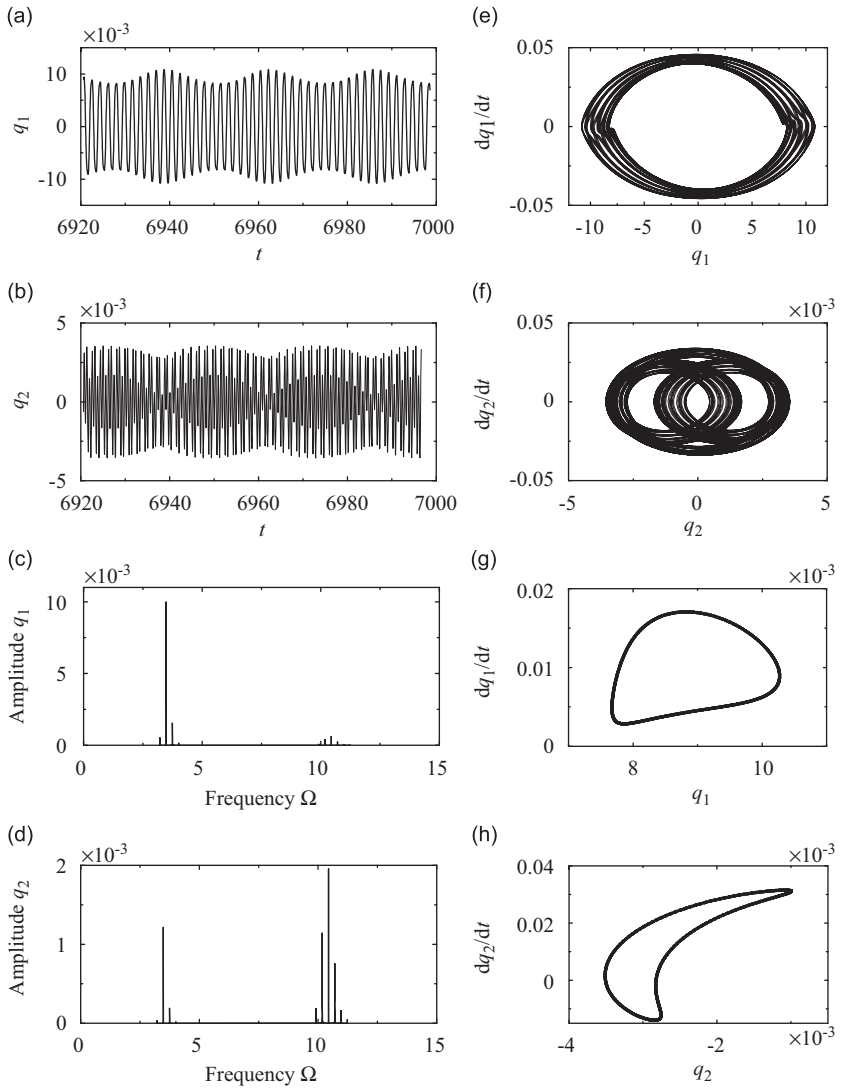

Fig. 4. Quasi-periodic response for the excitation frequency ratio $\Omega/\omega_1 = 1.2333$. (a, b) Time history; (c, d) Fourier spectrum; (e, f) phase plane and (g, h) Poincaré sections.

The following bifurcations near the internal resonance region '*E*–*F*' can be observed as the excitation frequency ratio sweeps from points '*E*' to '*F*': periodic→quasi-periodic→chaotic→periodic→quasi-periodic→periodic. As the excitation frequency ratio decreases from point '*F*', the system response results in a sequence of periodic→quasi-periodic or chaotic →periodic vibrations.

5.2. The case of Ω near ω_2

When the excitation frequency, Ω, is near the second natural frequency, ω_2, one should assume a zero value of f_1 and a nonzero value of f_2 in Eq. (26). Let $\tau = \Omega t = 3\tau_1$, where $\tau_1 \approx \omega_1 t$. The solutions of q_1 and q_2 in this case can be taken as

$$q_j = \sum_{k=1}^{n_c} a_{jk}\cos(2k-1)\tau_1 + \sum_{k=1}^{n_s} b_{jk}\sin(2k-1)\tau_1, \quad j = 1,2 \tag{29}$$

We again take $n_c = n_s = 8$, and the assumed solutions are simplified to be

$$q_1 = A_{11}\cos\tfrac{1}{3}(\tau+\phi_{11}) + A_{12}\cos(\tau+\phi_{12}) + \cdots, \tag{30}$$

$$q_2 = A_{21}\cos\tfrac{1}{3}(\tau+\phi_{21}) + A_{22}\cos(\tau+\phi_{22}) + \cdots \tag{31}$$

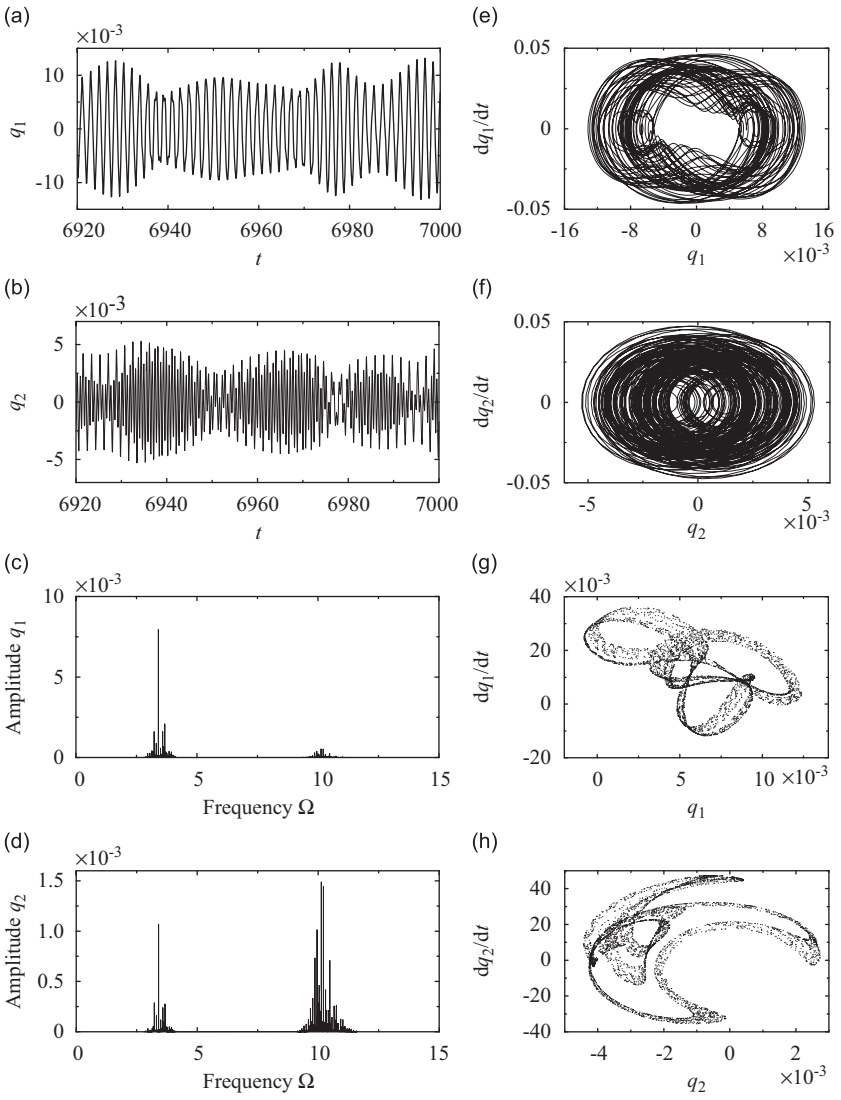

Fig. 5. Chaotic response for the excitation frequency ratio $\boldsymbol{\Omega}/\omega_1 = 1.2066$: (a, b) Time history; (c, d) Fourier spectrum; (e, f) phase plane and (g, h) Poincaré sections.

where

$$A_{jk} = \sqrt{a_{jk}^2 + b_{jk}^2}, \quad \phi_{jk} = \tan^{-1}(-b_{jk}/a_{jk}), \quad j = 1,2, \quad k = 1,2,\ldots,8,$$

There are two branches of solutions corresponding to Eqs. (30) and (31), which are A_{11}=A_{21}=0, and $A_{11}\neq 0$ and $A_{21}\neq 0$. Figs. 9(a), (b), and (c) show the frequency-response curves for $\boldsymbol{\Omega}/\omega_2 \sim A_{11}$, $\boldsymbol{\Omega}/\omega_2 \sim A_{22}(A_{11}\neq 0)$ and $\boldsymbol{\Omega}/\omega_2 \sim A_{22}(A_{11}=0)$, respectively, with f_2=0.0055 and μ_{11}=μ_{22}=0.04. One of the branches of the solution is A_{11}=A_{21}=0, as shown in Fig. 9(c), and the resulting oscillation in this case consists of only the second harmonic term in which the excitation frequency, Ω, is equal to the response frequency; i.e., the system response is in fundamental resonance with Ω near ω_2. The characteristic of A_{22} is similar to that of the single Duffing system that expresses the jump phenomena; however, internal resonance does not occur here. The other branch of the solution is the curve in which $A_{11}\neq 0$ and $A_{21}\neq 0$, as shown in Figs. 9(a, b), and the oscillation contains oscillatory components with frequency $\Omega/3$. It is found that the amplitude A_{11} is greater than amplitude A_{22} in most response regions. In other words, the system response is dominated by the first harmonic terms where the frequency is one-third of the excitation frequency, Ω. Hence, these resonance are called subharmonic resonances which are expressed by $\boldsymbol{\Omega}/\omega_2 \sim A_{11}$ and $\boldsymbol{\Omega}/\omega_2 \sim A_{22}$.

In Figs. 9(a, b), the subharmonic resonances, frequency-response curves acquired using the IHB method solutions, are similar to those for non-gyroscopic systems with cubic nonlinearities obtained in literature [24]. The system response curves are complex loops consisted of three stable portions, which compare very well with the steady solution obtained

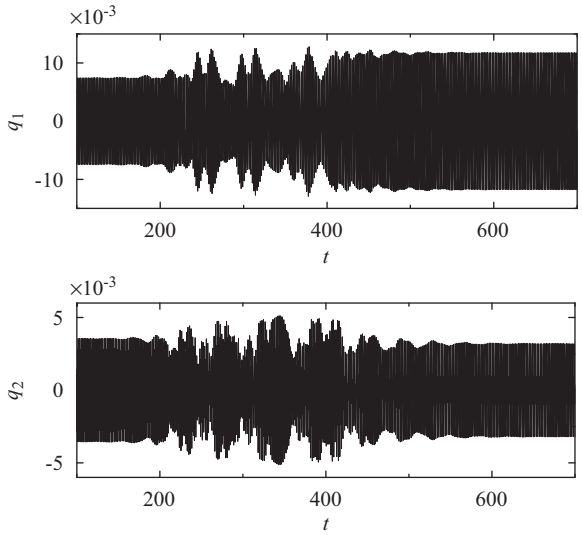

Fig. 6. Time history of the two modes q_1, q_2 at $\boldsymbol{\Omega}/\omega_1 = 1.1951$.

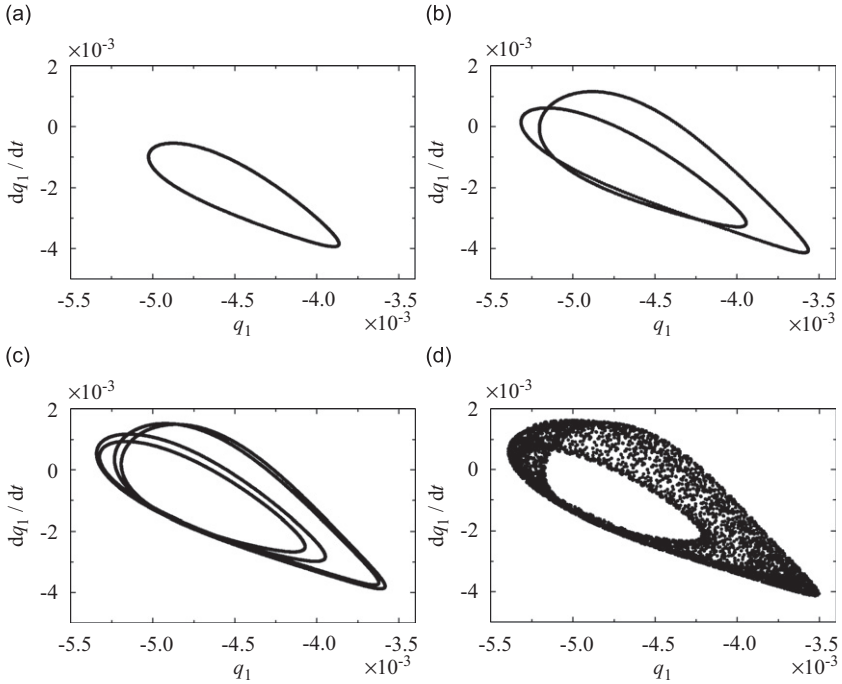

Fig. 7. Poincaré sections as increasing the excitation frequency ratio: (a) $\boldsymbol{\Omega}/\omega_1 = 1.16834$, (b) $\boldsymbol{\Omega}/\omega_1 = 1.16894$, (c) $\boldsymbol{\Omega}/\omega_1 = 1.16900$ and (d) $\boldsymbol{\Omega}/\omega_1 = 1.16911$.

from numerical integration. The first stable solution is generated at a saddle-node bifurcation point '*A*' ($\boldsymbol{\Omega}/\omega_2 = 1.0224$), and loses its stability at the other saddle-node bifurcation point '*B*' ($\boldsymbol{\Omega}/\omega_2 = 1.0816$). The second stable solution is generated at a saddle-node bifurcation point '*C*' ($\boldsymbol{\Omega}/\omega_2 = 1.0234$), and it loses its stability via a Hopf bifurcation point '*D*' ($\boldsymbol{\Omega}/\omega_2 = 1.0306$). The third stable solution is generated via a Hopf bifurcation point '*E*' ($\boldsymbol{\Omega}/\omega_2 = 1.1746$) and loses its stability at a saddle-node bifurcation '*F*' ($\boldsymbol{\Omega}/\omega_2 = 1.2280$).

As the excitation frequency ratio, Ω/ω_2, decreases from point '*E*' to 1.1648, there exists quasi-periodic vibration. Fig. 10 shows the time histories, Fourier spectra, phase plane diagrams and Poincaré sections for the excitation frequency ratio at $\boldsymbol{\Omega}/\omega_2 = 1.1694$, obtained from numerical integration. It is also shown that the beating phenomena occur in Figs. 10(a, b), and energy is continuously being exchanged between the two modes. For $\boldsymbol{\Omega}/\omega_2 = 1.1694$, the Fourier spectra consist of discrete components, phase plane portraits are banded attractors and Poincaré sections are closed curves, as shown in

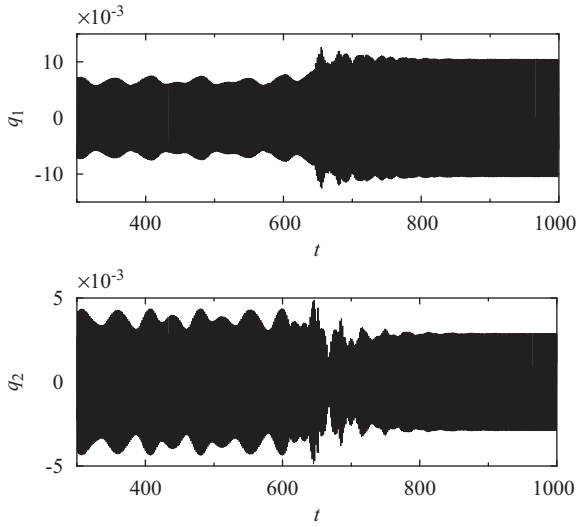

Fig. 8. Time history of the two modes q_1, q_2 at $\boldsymbol{\Omega}/\omega_1 = 1.16967$.

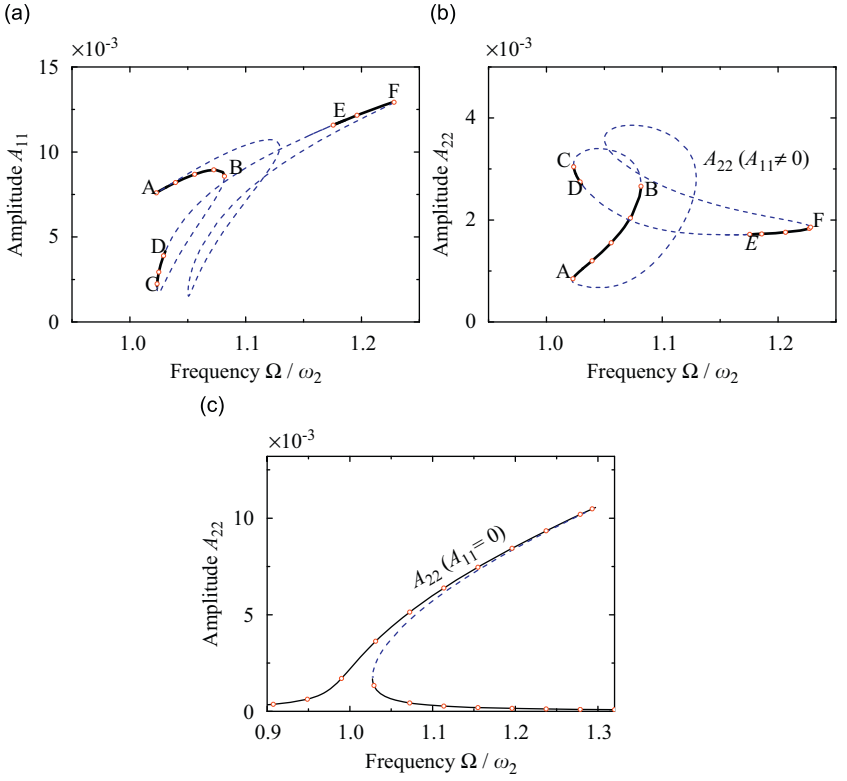

Fig. 9. Response curves as $\omega_2 \approx 3\omega_1, \boldsymbol{\Omega} \approx \omega_2$ with $f_2 = 0.0055, \mu_{11} = \mu_{22} = 0.04$: (a)$\boldsymbol{\Omega}/\omega_2 \sim A_{11}$, (b)$\boldsymbol{\Omega}/\omega_2 \sim A_{22}(A_{11} \neq 0)$ and (c) $\boldsymbol{\Omega}/\omega_2 \sim A_{22}(A_{11} = 0)$. ——— IHB stable, - - - - - IHB unstable; ○ numerical integration (NI).

Figs. 10(c–h). The largest Lyapunov exponents computed for the region from point '*E*' to 1.1648 are very small values, which can be taken to be zero for quasi-periodic vibration. As the excitation frequency ratio decreases slightly near 1.1648, the system response moves away from the quasi-periodic response and jumps to a stable periodic response. Fig. 11 shows the time history at $\boldsymbol{\Omega}/\omega_2 = 1.1646$. The amplitudes of the first and second modes (q_1 and q_2) drop for a finite period of time and then jumps to a stable periodic response of the second fundamental resonance.

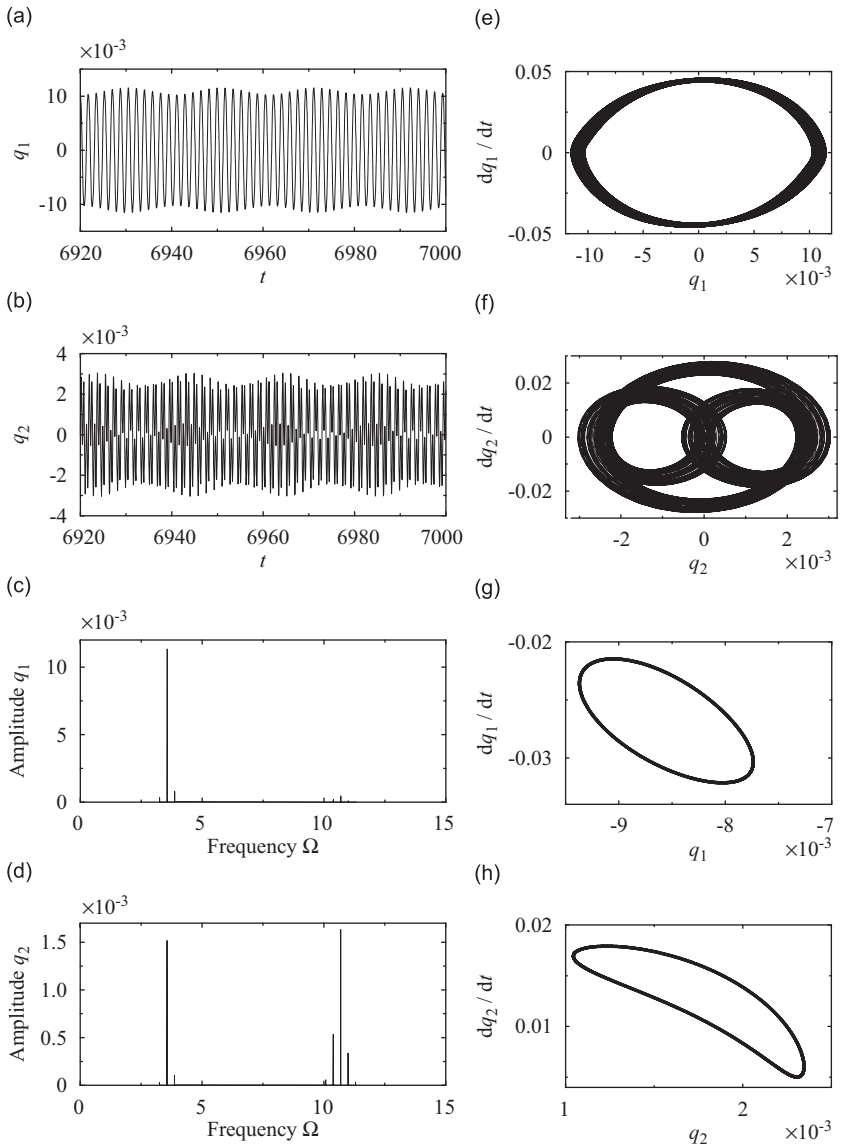

Fig. 10. Quasi-periodic response for the excitation frequency ratio $\boldsymbol{\Omega}/\omega_2 = 1.1694$: (a, b) Time history; (c, d) Fourier spectrum; (e, f) phase plane and (g, h) Poincaré sections.

A quasi-periodic response bifurcates into a chaotic response when Ω/ω_2 increases from the Hopf bifurcation point '*D*' to 1.0337. The stable response loses its stability via the Hopf bifurcation point 'D' and becomes a quasi-periodic vibration, as shown in Fig. 12(a). Then, the quasi-periodic vibration undergoes a sequence of period doubling bifurcations, as shown in Fig. 12(b) and (c), eventually resulting in chaotic vibration. The chaotic attractor is observed in Fig. 12(d), and the Lyapunov exponents computed for these parameter values are 0.00763, 5.24621×10^{-5}, -0.03647 and -0.05127. The largest Lyapunov exponent is positive, confirming its chaotic nature. As the excitation frequency ratio increases slightly near the boundary crises, the system response moves away from the chaotic attractor and jumps to a stable periodic response of the second fundamental resonance. In Fig. 13, we show the time history at $\boldsymbol{\Omega}/\omega_2 = 1.0341$. The two modes, q_1 and q_2, jump from a quasi-periodic vibration to a stable periodic vibration after a finite period of time, and the main response frequency of the first two modes, q_1 and q_2, change from $\omega_2/3$ to ω_2.

The following bifurcations near the internal resonance region '*E*–*F*' can be observed with a sweep of the excitation frequency ratio from point '*E*' to point '*F*': periodic → quasi-periodic → chaotic → periodic vibrations. As the excitation frequency ratio decreases from point '*F*', the system response results in a sequence of periodic → quasi-periodic → periodic vibrations.

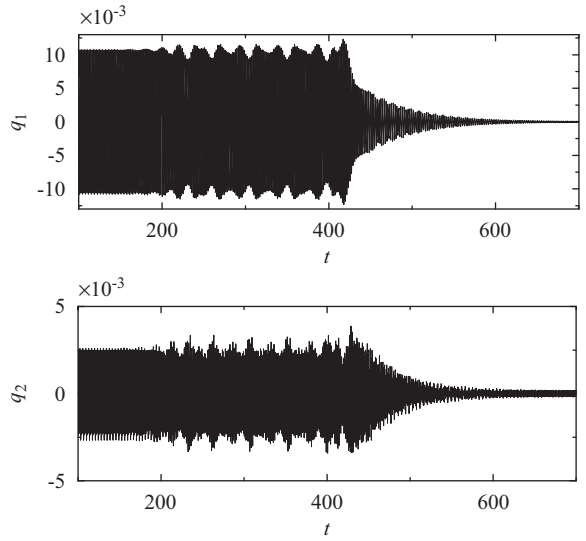

Fig. 11. Time history of the two modes q_1, q_2 at $\Omega/\omega_2 = 1.646$.

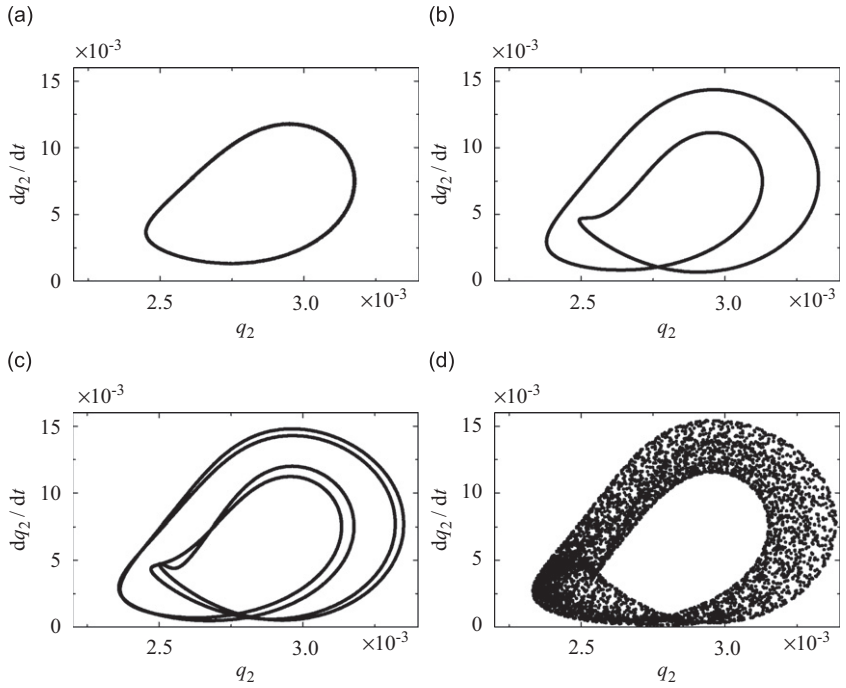

Fig. 12. Poincaré sections: (a) Ω/ω_2=1.03283, (b) Ω/ω_2=1.03324, (c) Ω/ω_2=1.03341 and (d) Ω/ω_2=1.03365.

6. Conclusions

The transverse nonlinear steady-state vibrations of the axially moving beam with a three-to-one internal resonance between the first two modes, subjected to a harmonic excitation, have been investigated using the IHB method. The Floquet theory was used to analyze the stability of periodic solutions and help determine the bifurcation points. The characteristics of quasi-periodic or chaotic response in terms of the time histories, phase plane plots, Pioncaré sections, Fourier spectra and Lyapunov exponents were treated numerically.

The periodic solutions, including fundamental resonance and subharmonic resonance obtained from the IHB method, match very well with the numerically integrated solutions. The response curves of the axially moving beam show hardening-spring nonlinear characteristics. For fundamental resonances of the first and second modes, the response curves

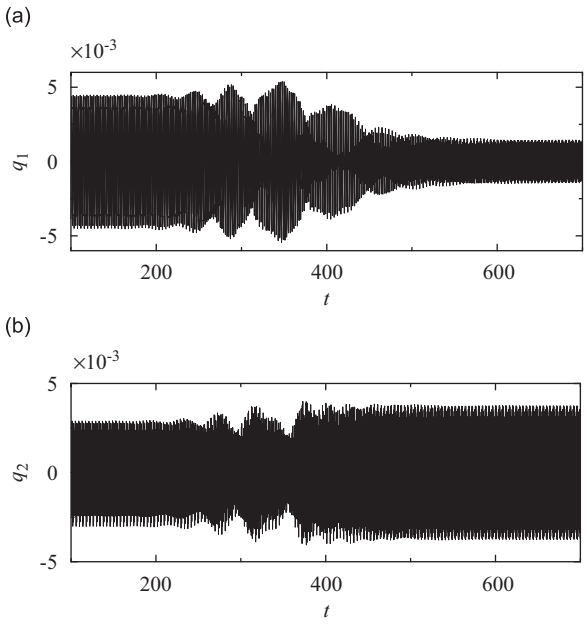

Fig. 13. Time history of the two modes q_1, q_2 at $\boldsymbol{\Omega}/\omega_2 = 1.0341$.

are similar to a single Duffing system, while for subharmonic resonance of the second mode, the response curve is in a closed form.

When the excitation frequency, Ω, is close to the first two natural frequencies, ω_1 and ω_2, quasi-periodic and chaotic responses are found in some regions in which the energy is continuously being exchanged between the two modes. By sweeping the excitation frequency, the axially moving beam vibrations possess complex vibrations including jump responses and the coexistence of multiple attractors, quasi-periodic to chaotic attractors and boundary crisis.

Acknowledgements

Financial supports from the National Natural Science Foundation of China (11002164 and 10972240) and Research Grants Council of Hong Kong SAR (Project no. HKU7102/08E) are gratefully acknowledged.

References

[1] A.G. Ulsoy, C.D. Mote Jr., R. Syzmani, Principal developments in band saw vibration and stability research, *Holz als Roh-und Werkstoff* 36 (1978) 273–280.
[2] J.A. Wickert, C.D. Mote Jr., Current research on the vibration and stability of axially-moving materials, *Shock and Vibration Digest* 20 (1988) 3–13.
[3] J.A. Wickert, C.D. Mote Jr., Classical vibration analysis of axially moving continua, *Journal of Applied Mechanics* 57 (1990) 738–744.
[4] J.A. Wickert, Non-linear vibration of a traveling tensioned beam, *International Journal of Non-Linear Mechanics* 27 (1992) 503–517.
[5] F. Pellicano, F. Vestroni, Nonlinear dynamics and bifurcations of an axially moving beam, *Journal of Vibration and Acoustics* 122 (2000) 21–30.
[6] F. Pellicano, F. Vestroni, Complex dynamics of high-speed axially moving systems, *Journal of Sound and Vibration* 258 (2002) 31–44.
[7] F. Pellicano, A. Fregolent, A. Bertuzzi, F. Vestroni, Primary and parametric non-linear resonance of a power transmission belt: experimental and theoretical analysis, *Journal of Sound and Vibration* 244 (2001) 669–684.
[8] H.R. Öz, M. Pakdemirli, H. Boyacm, Non-linear vibrations and stability of an axially moving beam with time-dependent velocity, *International Journal of Non-Linear Mechanics* 36 (2001) 107–115.
[9] H.R. Öz, Non-linear vibrations and stability analysis of tensioned pipes conveying fluid with time-dependent velocity, *International Journal of Non-Linear Mechanics* 36 (2001) 1031–1039.
[10] L.Q. Chen, X.D. Yang, Stability in parametric resonance of axially moving viscoelastic beams with time-dependent velocity, *Journal of Sound and Vibration* 284 (2005) 879–891.
[11] L.Q. Chen, X.D. Yang, Steady-state response of axially moving viscoelastic beams with pulsating speed: comparison of two nonlinear models, *International Journal of Solids and Structures* 42 (2005) 37–50.
[12] K.Y. Sze, S.H. Chen, J.L. Huang, The incremental harmonic balance method for nonlinear vibration of axially moving beams, *Journal of Sound and Vibration* 281 (2005) 611–626.
[13] S.L. Lau, Y.K. Cheung, Amplitude incremental variational principle for nonlinear structural vibrations, *Journal of Applied Mechanics—Transactions of the ASME* 48 (1981) 959–964.
[14] Y.K. Cheung, S.L. Lau, Incremental time–space finite strip method for nonlinear structural vibrations, *Earthquake Engineering and Structural Dynamics* 10 (1982) 239–253.
[15] S.L. Lau, Y.K. Cheung, S.Y. Wu, A variable parameter incremental method for dynamic instability of linear and nonlinear elastic systems, *Journal of Applied Mechanics—Transactions of the ASME* 49 (1982) 849–853.
[16] C.M. Chin, A.H. Nayfeh, Three-to-one internal resonances in hinged–clamped beams, *Nonlinear Dynamics* 12 (1997) 129–154.

[17] A. Abe, Y. Kobayashi, G. Yamada, Two-mode response of simply supported, rectangular laminated plates, *International Journal of Non-Linear Mechanics* 33 (1998) 675–690.
[18] C.H. Riedel, C.A. Tan, Coupled, forced response of and axially moving strip with internal resonance, *International Journal of Non-Linear Mechanics* 37 (2002) 101–116.
[19] G. Suweken, W.T. Van Horssen, On the transversal vibrations of a conveyor belt with a low and time-varying velocity. II: the beam-like case, *Journal of Sound and Vibration* 267 (2003) 1007–1027.
[20] P. Friedmann, C.E. Hammond, T.H. Woo, Efficient numerical treatment of periodic systems with application to stability problems, *International Journal for Numerical Methods in Engineering* 11 (1977) 1117–1136.
[21] C.S. Hsu, Impulsive parametric excitation: theory, *Journal of Applied Mechanics—Transactions of the ASME* 39 (1972) 551–558.
[22] C.S. Hsu, On approximating a general linear periodic system, *Journal of Mathematical Analysis and Applications* 45 (1974) 234–251.
[23] C.S. Hsu, W.H. Cheng, Applications of the theory of impulsive parametric excitation and new treatments of general parametric excitation problems, *Journal of Applied Mechanics—Transactions of the ASME* 40 (1973) 78–86.
[24] Y.K. Cheung, S.H. Chen, S.L. Lau, Application of the incremental harmonic balance method to cubic non-linearity systems, *Journal of Sound and Vibration* 140 (1990) 273–286.